

Simple BODIPY dyes as suitable electron-donors for organic bulk heterojunction photovoltaic cells

António Aguiar^a, Joana Farinhas^b, Wanderson da Silva^a, Maria Susano^c, Manuela Ramos Silva^c, Luís Alcácer^b, Santosh Kumar^a, Christopher M.A. Brett^a, Jorge Morgado^{b,d}, Abílio J.F.N. Sobral^{a,*}

^a Chemistry Department, FCTUC, University of Coimbra, 3004-535, Coimbra, Portugal

^b Instituto de Telecomunicações, Instituto Superior Técnico, Av. Rovisco Pais 1, P-1049-001, Lisboa, Portugal

^c CFisUC, Department of Physics, University of Coimbra, 3004-516, Coimbra, Portugal

^d Department of Bioengineering, Instituto Superior Técnico, University of Lisbon, Av. Rovisco Pais 1, P-1049-001, Lisboa, Portugal

ARTICLE INFO

Keywords:

BODIPY dyes
Small molecules
Optoelectronic properties
Organic photovoltaic cells
Photovoltaic performance

ABSTRACT

In this work we present the synthesis and characterization (including the report of two new crystal structures) of a series of *meso*-substituted boron-dipyrromethene (BODIPY) molecules. With an accessible synthesis, these simple BODIPYs have characteristics that par with those BODIPYs having more complex structures, what makes them very interesting materials for industrial production. The photovoltaic performance of the synthesized BODIPYs was evaluated in bulk heterojunction organic solar cells, where they were used as electron-donors. We found that the presence of electron-withdrawing groups has a detrimental effect on the photovoltaic performance, while the *meso*-free structure shows an improved efficiency in comparison with the *meso*-substituted BODIPYs. We also studied the origin of the *meso*-unsubstituted derivative, elucidating at least one of its formation processes, which can open a new way of BODIPY synthesis.

1. Introduction

The photovoltaic market is still ruled by the silicon-based solar cells due to their good efficiency and high stability, supported by the well-established modern inorganic semiconductors technology [1,2]. However, high costs, prospects for building integration and environmental concerns about this industry have driven the research into alternative organic photovoltaic technologies, such as, dye-sensitized solar cells and fully organic photovoltaic cells (OPVs). In fact, OPV are now emerging as one of the most viable alternatives due to their low-cost production, mechanical flexibility and lightweight [2–4].

The organic photovoltaic effect starts by sunlight absorption that promotes electron excitations of the organic material (absorber) forming excitons (bound electron-hole pairs). In order to generate free charges (free electrons and holes) those excitons need to be split. This splitting is achieved by combination with another material that has an adequate energy offset of the frontier orbitals (HOMO and LUMO). The combination of such materials can be made in a bi-layer or in a blend (commonly known as bulk heterojunction (BHJ)), which is the most used approach. Its main particularity is that the active layer presents an interpenetrated biphasic network of the electron-donor and the electron-acceptor organic semiconductors [5,6].

Many new small molecules and conjugated polymers have been designed and developed for organic solar cells. Initially, polymers were the most tested and efficient materials, but today solar cells based on small molecules show similar, or even better performance, than those based on polymers [7]. Small molecules show smaller batch-to-batch variations and well-defined absorption spectra due to their uniform and defined molecular structures.

Boron-dipyrromethene (BODIPY) molecules constitute an important class of visible light absorbing dyes, with a wide variety of applications [8–14]. BODIPYs are auspicious photosensitizer materials for OPVs due to their properties, such as photochemical and chemical stability, high molar absorption coefficients, excitation/emission wavelengths in the visible and NIR spectral region, good solubility in inorganic solvents and ease of functionalization [15–17]. Despite this, research efforts still remain at a low level if compared with other pyrrolic small molecules like porphyrins or phthalocyanines.

In fact there is a relatively low number of published works relating BODIPY with OPV systems [9,10]. Since the first published data on BODIPY with OPVs in 2009 [18], there are only a few reports showing power conversion efficiencies (PCE) above 3% [9,10], being the highest PCE reported for BODIPY small molecule-based photovoltaic cells of 7.2% [19]. Generally, the BODIPYs used in OPV are complex α - or β -

* Corresponding author.

E-mail address: asobral@ci.uc.pt (A.J.F.N. Sobral).

<https://doi.org/10.1016/j.dyepig.2019.107842>

Received 27 May 2019; Received in revised form 22 July 2019; Accepted 26 August 2019

Available online 27 August 2019

0143-7208/ © 2019 Elsevier Ltd. All rights reserved.

functionalized BODIPYs and the most used methods to prepare such derivatives are either the Sonogashira reaction or the Suzuki coupling [20–23]. The preparation of those BODIPYs involves several synthetic steps that increase the cost of the final product. On the other hand, “simple” BODIPYs i.e. BODIPY made in a one pot reaction without any post-functionalization were never reported as electron-donor and, consequently, their photovoltaic performance was not yet described.

In this work, we present the synthesis, characterization and application as electron-donor materials in OPVs of a series of very simple *meso*-substituted BODIPYs made in a one-pot process. This work demonstrates that simple BODIPYs can achieve very high open circuit voltages and we propose that these results can be used as “standards” for more complex BODIPYs in order to avoid elaborated synthesis that do not bring significant PCE improvements. We also clarified the appearance of a common contaminant in most of the previously reported BODIPYs synthesis. The isolation of that BODIPY by-product (*meso*-free BODIPY) allowed us to discover that its photovoltaic properties are significant, and consequently, it is possible that previous studies may have been unintentionally disturbed by this contaminant. Our findings on the origin of this *meso*-free BODIPY may be used in a new synthetic method (acid free/aldehyde free) for BODIPYs.

2. Experimental

2.1. Materials and reagents

Reagents and solvents were obtained from Sigma-Aldrich and used without further purification. Solvents for photophysical studies were HPLC grade (CHROMASOLV plus) purchased from Sigma-Aldrich. Analytical thin layer chromatography (TLC) was performed on Merck silica gel plates with F-254 indicator. For visualization, a twin wavelength ultraviolet lamp (254 and 365 nm) was used. Silica gel column chromatography was carried out with silica gel (230–400 mesh) from Fluka.

2.2. Equipments

Reagents and solvents were obtained from Sigma-Aldrich and used without further purification. Solvents for photophysical studies were HPLC grade (CHROMASOLV plus) purchased from Sigma-Aldrich. The fullerene PC₆₀BM was purchased from Sigma-Aldrich. Analytical thin layer chromatography (TLC) was performed on silica gel plates with F-254 indicator (Merck). Visualization was accomplished by a twin wavelength ultraviolet lamp (254 and 365 nm). Silica gel column chromatography was carried out with silica gel (230–400 mesh) from Fluka.

¹H, ¹⁹F and ¹³C spectra were recorded on a Bruker AVANCE III NMR (operating at 400.15 MHz for proton, 100.63 MHz for carbon and 376 MHz for fluorine) with CDCl₃ as solvent. Chemical shifts (δ) are quoted in ppm relative to TMS. Coupling constants (J) are presented in Hz. High-performance liquid chromatography (HPLC) analysis was performed using a Dionex Ultimate 3000 system equipped with an auto-injector and an Hichrom 5C₁₈ column (15 cm \times 5 mm \times 4.6 mm). The experiments were performed at 30 °C with acetonitrile:H₂O (8:2) as isocratic eluent with a volume of injection of 10 μ l and at flow rate of 0.8 cm³/min.

High-resolution ESI positive mode mass spectra were obtained on a QqTOF Impact II™ mass spectrometer (Bruker Daltonics) operating in the high-resolution mode. Samples were analyzed by flow injection analysis (FIA) using an isocratic gradient 30 A:70 B of 0.1% formic acid in water (A) and 0.1% of formic acid in acetonitrile (B), at a flow rate of 10 μ l min⁻¹ over 15 min. The TOF analyser was calibrated in the *m/z* range 100–1500 using an internal calibration standard (Tune mix solution) which is supplied from Agilent. The full scan mass spectra were acquired over a mass range of 100–1350 *m/z* at a spectra rate of 1 Hz.

Electronic absorption spectra were recorded on a Jasco V-530 double-beam UV/Vis spectrometer, using 1 cm path length quartz cells. Steady-state fluorescence studies were recorded in a Horiba-Jobin-Yvon SPEX Fluorlog 3-22 spectrometer, using dilute solutions and were

Table 1

BDP6 synthesis using 5 ml of solvent, 1 mmol of 3-ethyl-2,4-dimethylpyrrole, 1 eq. of DDQ and 17eq. of boron trifluoride etherate and 12 eq. diisopropylamine. Trifluoro acetic acid (20 μ l) was used when shown.

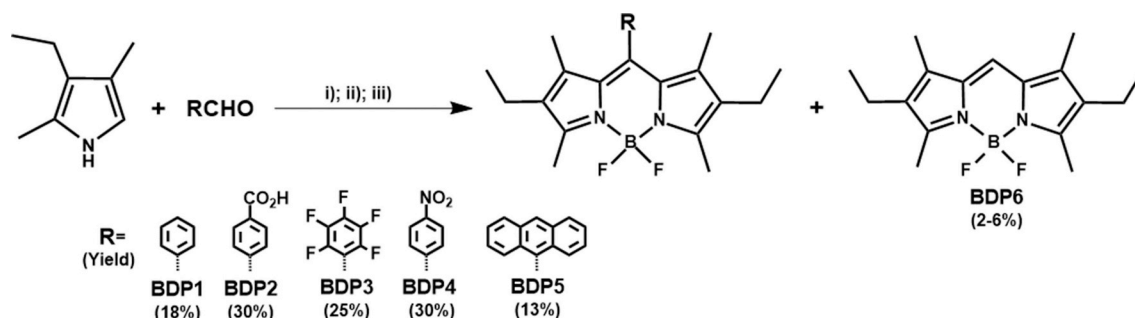
Solvent	TFA	BDP6 yield
CH ₂ Cl ₂	yes	4%
CH ₂ Cl ₂	no	4%
CH ₂ I ₂	no	8%
CH ₂ Br ₂	no	4%

automatically corrected for the wavelength response of the system. Fluorescence quantum yields were calculated by a comparative method using rhodamine 6G (Φ_F (470–555 nm) = 0.88 in ethanol) as reference. Cyclic voltammetric (CV) measurements were carried out with a computer controlled Ivium Compact Stat, with a one-compartment three electrode system consisting of a glassy carbon electrode (GCE) (geometric area of 0.00785 cm²) as working electrode, a platinum wire as counter electrode and an Ag/AgCl (3 M KCl) reference electrode, at a scan rate of 50 mVs⁻¹. Tetrabutylammonium tetrafluoroborate (TBATFB, 0.1 M) in dichloroethane was used as supporting electrolyte. The results were calibrated using a 1 mM ferrocene/ferrocenium (Fc/Fc⁺) redox couple as internal standard. It is assumed that the redox potential of Fc/Fc⁺ has an absolute energy level of –4.80 eV to vacuum. CV experiments were carried out using 1 mM concentrations of each BODIPY. UV/Vis absorption spectra of the films were recorded in a Cecil 7200 spectrophotometer. The HOMO/LUMO calculations were performed with the basis set split valence, increased with polarization function type (d) 6-31G*, using the SPARTAN v.10 software package (Spartan, Wave Function Inc. USA).

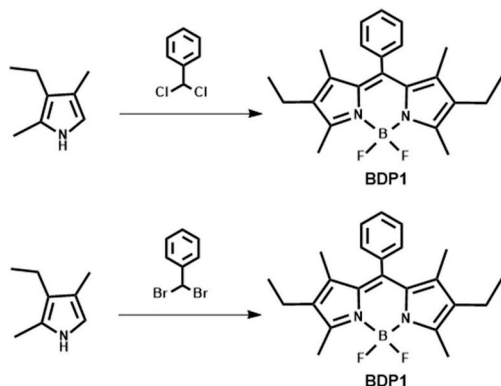
Single-crystal X-ray diffraction studies of **BDP4** and **BDP5** were carried out on a Bruker APEXII diffractometer using MoK α radiation. Data reduction was performed with SMART and SAINT software [24]. Lorentz and polarization corrections were applied. A multi-scan absorption correction was applied using SADABS [25]. The structure was solved by direct methods using SHELXS-97 program and refined on F₂s by full-matrix least-squares with SHELXL-97 program [26]. The anisotropic displacement parameters for non-hydrogen atoms were applied. The hydrogen atoms were placed at calculated positions and refined with isotropic parameters as riding atoms. One of the two non-equivalent molecules of **BDP4** shows signs of disorder and DFIX constraints had to be used.

Film thicknesses were measured with a Dektak 6 M profilometer. The surface topography of the films was characterized by Atomic Force Microscopy using a Nano Observer Microscope from Concept Scientific Instruments (Les Ulis, France). All images were taken with 256 \times 256 pixels resolution and processed with Gwyddion (version 2.26) software.

The photovoltaic devices were prepared on glass substrates coated with 100 nm thick indium-tin oxide (ITO), cleaned under ultrasounds with distilled water and a non-ionic detergent (Derquim Im 02 neutral phosphate free) followed by washing with distilled water, acetone, isopropyl alcohol and then dried under a N₂ stream. The ITO surface was then treated with UV-oxygen plasma for 3 min prior to depositing, by spin coating, a 40 nm layer of poly (3,4-ethylenedioxythiophene):polystyrene sulfonic acid (PEDOT:PSS) (Clevios P VP.AI 4083, from Heraeus), which was then dried on a hot plate at 125 °C for 10 min. The solutions of the blends were spin-coated (1300 rpm, 60 s) on top of the PEDOT:PSS in air. Following the spin coating of the active blends, Ca (20 nm) and Al (80 nm) were thermally evaporated on top, under a base pressure of 10⁻⁶ mbar, defining a device area of 0.24 cm². The current-voltage curves of the photovoltaic cells were measured under inert atmosphere (N₂) using a Keithley 2400 Source-Meter unit. The curves under illumination were measured with a solar simulator with simulated AM1.5G illumination at 88 mW/cm² (Oriol Sol 3A, 69920, Newport). At least 16 devices of each series were prepared. The light intensity of the solar simulator was verified using a calibrated solar cell. External quantum efficiency (EQE) spectra were obtained under short-circuit conditions, using a homemade system with a halogen lamp as light



Scheme 1. General procedure for the preparation of the BODIPY series: i) TFA; ii) DDQ; iii) diisopropylethylamine, $\text{BF}_3 \cdot \text{O}(\text{C}_2\text{H}_5)_2$.



Scheme 2. Synthesis of **BDP1** using α,α -dichlorotoluene and α,α -dibromotoluene (1 mmol of 3-ethyl-2,4-dimethylpyrrole, 1 eq. of DDQ and 17 eq. of boron trifluoride etherate and 12 eq. diisopropylamine).

source coupled to a monochromator. Its intensity at each wavelength was determined using a calibrated photodiode. The short-circuit current was measured with a Keithley 2400 Source-Meter.

2.3. Synthesis

BDP1, **BDP2**, **BDP3**, **BDP4** and **BDP5** were prepared according to procedures described previously, using benzaldehyde, 4-formylbenzoic acid, pentafluorobenzaldehyde, 4-nitrobenzaldehyde and 9-

Table 3

Conformation of the ethyl groups, length of the bond between the *meso*-carbon and the substituent and the dihedral angle between the least-squares plane of the substituent and that of the central core.

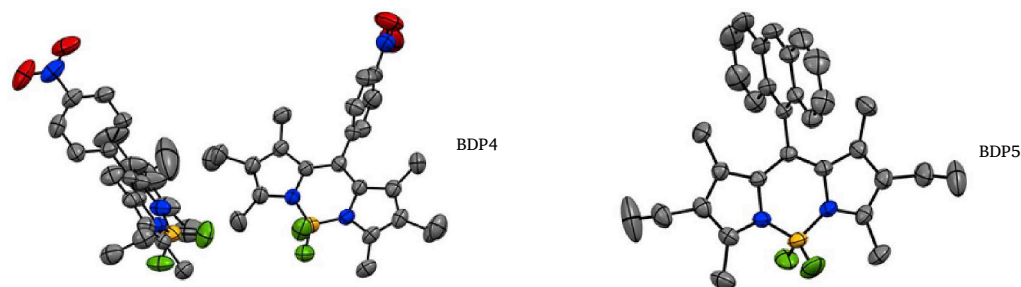
Entries	Conformation	Bond length (Å)	Dihedral angle (°)
FIDLIP [32]	<i>trans</i>	1.514 (3)	89.41 (8)
UNIFIG [33]	<i>trans</i> ; <i>cis</i> ; <i>trans</i>	1.478(10); 1.515(10); 1.475 (10)	78.2(2); 78.8(2); 84.5(2)
BDP4	<i>trans</i> ; <i>trans</i>	1.486(3); 1.482(3)	87.87(6); 89.89(7)
BDP5	<i>trans</i>	1.495 (2)	89.99 (5)
XODGUT [29]	<i>cis</i>	–	–

anthracenecarboxyaldehyde, respectively, as the aldehyde reagents [27]. 3-Ethyl-2,5-dimethyl-pyrrole (0.75 ml, 5.5 mmol) and the aldehyde (2.75 mmol) were added to dried, freshly distilled dichloromethane (50 ml) and the solution was stirred for 20 min under a flux of N_2 . Then, trifluoroacetic acid was added (1 drop) and the mixture was stirred overnight under N_2 atmosphere, at room temperature. After that, 2,3-dichloro-5,6-dicyanobenzoquinone (1 eq.) was added to the reaction mixture, and this was stirred overnight, under N_2 atmosphere, at room temperature. Then N, N-diisopropylethylamine (12 eq.) and $\text{BF}_3 \cdot \text{Et}_2\text{O}$ (17 eq.) were added to the reaction mixture, and the reaction was left under inert atmosphere with slow stirring overnight, at room temperature. After that, washing was made with water and brine, followed by solvent evaporation under reduced pressure. **BDP6** is a by-product of the **BDP1** to **BDP5** syntheses. It can also be synthesized using the same protocol but

Table 2

Oak Ridge Thermal Ellipsoid Plot (ORTEP) drawing of the molecular structures Ellipsoids at 50% probability level of the **BDP4** and **BDP5** structures and crystal data details. Hydrogen atoms were omitted for clarity reasons.

Crystal data



Chemical formula	C23H26 B F2 N3 O2	C31H31 B F2 N2
M_r	425.28	480.39
Crystal system, space group	Triclinic, P-1	Triclinic, P-1
Temperature (K)	273	273
a, b, c (Å)	11.6249(3), 13.6843(4), 14.2855(3)	11.2904(4), 11.5999(4), 12.6196(4)
α, β, γ (°)	83.8040(10), 86.0120(10), 81.1080(10)	82.7320(17), 81.7817(15), 62.8494(13)
V (Å ³)	2228.86 (10)	1452.01 (9)
Z	2	2
Radiation type	Mo $K\alpha$	Mo $K\alpha$
μ (mm ⁻¹)	0.092	0.072

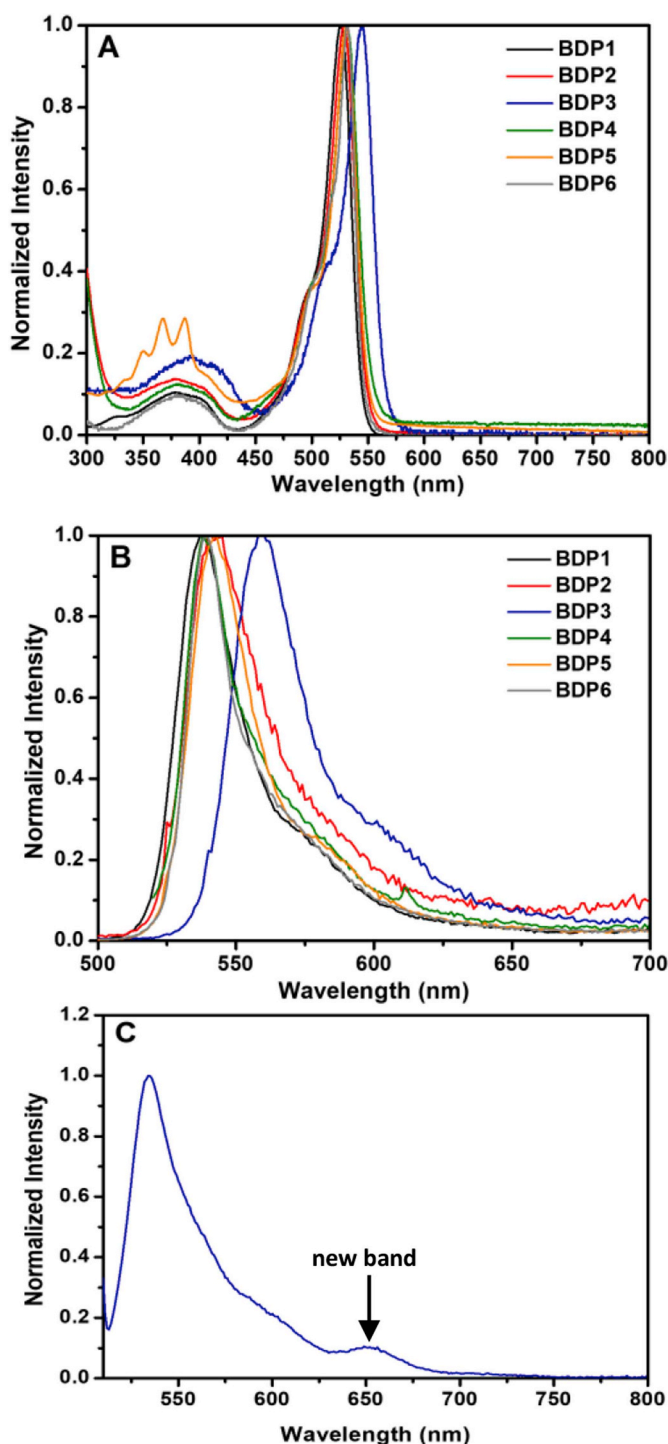


Fig. 1. Normalized absorption (A) and emission (B) spectra of BODIPY series in chloroform solution; Emission spectrum of BDP4 in acetonitrile solution (C).

without aldehyde. Further details on the synthesis of BDP6 are presented in Table 1. For the BDP2, BDP3 and BDP4 preparation reaction, the residue was chromatographed on silica gel using CH_2Cl_2 /petroleum ether (1:1) as eluent to separate BDP6 from the others. Preparative thin layer chromatography is necessary to separate BDP6 from BDP1 or BDP5. We used toluene as eluent and 20×20 cm silica gel 60 plates, with fluorescent indicator at 254 nm, from Fluka.

BDP1: Yield 18% (BDP1) 5% (BDP6); ^1H NMR (400 MHz, CDCl_3) (Electronic Supplementary Information (ESI) Fig. S2) δ (ppm): 7.49–7.45 (m; 3H); 7.30–7.26 (m; 2H); 2.53 (s, 6H), 2.30 (q, $J = 8$ Hz, 4H), 1.26 (s, 6H), 0.98 (t, $J = 8$ Hz, 6H); ^{19}F NMR (376 MHz, CDCl_3)

(ESI Fig. S3) δ (ppm): 145.80 (q, $J = 33.8$ Hz, 2F); ^{13}C NMR (100 MHz, CDCl_3) (ESI Fig. S4) δ (ppm): 153.68; 140.20; 138.42; 135.81; 132.77; 130.79; 129.01; 128.73; 128.28; 17.08; 14.62; 12.50; 11.62; HRMS (ESI Fig. S20) m/z $[\text{M} + \text{H}]^+$ calculated for $\text{C}_{23}\text{H}_{28}\text{BF}_2\text{N}_2^+$: 381.2308; Found: 381.2312;

BDP2: Yield 30% (BDP2) 2% (BDP6); ^1H NMR (400 MHz, CDCl_3) (ESI Fig. S5) δ (ppm): 8.25 (d; $J = 8.22$ Hz, 2H); 7.45 (d; $J = 8.22$ Hz, 2H); 2.54 (s, 6H), 2.37 (q, $J = 8$ Hz, 2F), 1.27 (s, 6H), 0.99 (t, $J = 8$ Hz, 6H); ^{19}F NMR (376 MHz, CDCl_3) (ESI Fig. S6) δ (ppm): 146.30 (q, $J = 33.8$ Hz, 2F) ^{13}C NMR (100 MHz, CDCl_3) (ESI Fig. S7) δ (ppm): 167.24; 154.17; 139.99; 138.55; 133.32; 132.05; 130.62; 129.24; 16.81; 14.34; 12.18; 11.49. HRMS (ESI Fig. S21) m/z $[\text{M} + \text{H}]^+$ calculated for $\text{C}_{24}\text{H}_{28}\text{BF}_2\text{N}_2\text{O}_2^+$: 425.2206; Found: 425.2205;

BDP3: Yield 25% (BDP3) 3% (BDP6); ^1H NMR (400 MHz, CDCl_3) (ESI Fig. S8) δ (ppm): 2.54 (s, 6H), 2.33 (q, $J = 8$ Hz, 4H), 1.51 (s, 6H), 1.02 (t, $J = 8$ Hz, 6H) ^{19}F NMR (376 MHz, CDCl_3) (ESI Fig. S9) δ (ppm): 139.23 (dd, $J = 22.6$, 11.3 Hz, 2F), 145.74 (q, $J = 33.8$ Hz, 2F), 151.11 (t, $J = 22.6$ Hz, 1F), 159.89 (m, $J = 22.6$, 11.3 Hz, 2F); ^{13}C NMR (100 MHz, CDCl_3) (ESI Fig. S10) δ (ppm): 156.15; 144.2 (d, $J = 250.52$ Hz); 141.94 (d, $J = 262$ Hz); 138.19 (d, $J = 257.86$ Hz); 136.58; 133.91; 130.36; 121.16; 110.32 (td, $J = 19.44$, 4.03 Hz); 17.09; 14.54; 12.74 (t, $J = 2.57$ Hz); 10.85. HRMS (ESI Fig. S22) m/z $[\text{M} + \text{H}]^+$ calcd for $\text{C}_{23}\text{H}_{22}\text{BF}_7\text{N}_2^+$: 471.1842; Found: 471.1842;

BDP4: Yield 30% (BDP4) 4% (BDP6); ^1H NMR (400 MHz, CDCl_3) (ESI Fig. S11) δ (ppm): 8.37 (d, $J = 8$ Hz, 2H); 7.53 (d, $J = 8$ Hz, 2H); 2.54 (s, 6H), 2.30 (q, $J = 8$ Hz, 4H), 1.26 (s, 6H), 0.98 (t, $J = 8$ Hz, 6H); ^{19}F NMR (376 MHz, CDCl_3) (ESI Fig. S12) δ (ppm): 145.76 (q, $J = 33.8$ Hz, 2F) ^{13}C NMR (100 MHz, CDCl_3) (ESI Fig. S13) δ (ppm): 155.00; 148.24; 142.90; 137.68; 136.81; 133.52; 129.93; 124.97; 17.08; 14.57; 12.62; 12.01. HRMS (ESI Fig. S23) m/z $[\text{M} + \text{H}]^+$ calculate for $\text{C}_{23}\text{H}_{27}\text{BF}_2\text{N}_3\text{O}_2^+$: 426.2159; Found: 421.2162;

BDP5: Yield 13% (BDP5) 6% (BDP6); ^1H NMR (400 MHz, CDCl_3) (ESI Fig. S14) δ (ppm): 8.56 (s, 1H); 8.03 (dd, $J = 8, 7, 1.0$ Hz, 2H); 7.45 (m, 4H); 6.94 (s, 1H); 2.60 (s, 6H), 2.18 (q, $J = 8$ Hz, 4H), 0.89 (t, $J = 8$ Hz, 6H) 0.55 (s, 6H); ^{19}F NMR (376 MHz, CDCl_3) (ESI Fig. S15) δ (ppm): 145.57 (q, $J = 33.8$ Hz, 2F) ^{13}C NMR (100 MHz, CDCl_3) (ESI Fig. S16) δ (ppm): 154.02; 138.14; 132.70; 131.35; 129.94; 129.27; 129.05; 128.29; 128.03; 126.77; 125.71; 125.51; 17.02; 14.58; 12.66; 10.54. HRMS (ESI Fig. S24) m/z $[\text{M} + \text{H}]^+$ calculated for $\text{C}_{31}\text{H}_{32}\text{BF}_2\text{N}_2^+$: 481.2621; Found: 481.2624;

BDP6: ^1H NMR (400 MHz, CDCl_3) (ESI Fig. S17) δ (ppm): 6.94 (s; 1H); 2.49 (s, 6H), 2.37 (q, $J = 8$ Hz, 4H), 2.16 (s, 6H), 1.06 (t, $J = 8$ Hz, 6H); ^{19}F NMR (376 MHz, CDCl_3) (ESI Fig. S18) δ (ppm): 146.31 (q, $J = 33.8$ Hz, 2F) ^{13}C NMR (100 MHz, CDCl_3) (ESI Fig. S19) δ (ppm): 153.63; 135.62; 131.40; 130.60; 117.55; 16.26; 13.56; 11.51 (t, $J = 2.20$ Hz); 8.35. HRMS (ESI Fig. S25) m/z $[\text{M} + \text{H}]^+$ calculated for $\text{C}_{17}\text{H}_{24}\text{BF}_2\text{N}_2^+$: 305.1995; Found: 305.2000;

3. Results and discussion

3.1. Synthesis

The series of BODIPYs presented in Scheme 1 was synthesized by the common method of acid catalyzed condensation of aromatic aldehydes and α -free-pyrroles, followed by the DDQ oxidation step and finished with the complexation with borontrifluoride, in the presence of a base [9,15,27].

All HPLC analyses for purity assessment were performed on a C18 reversed phase column (80% of acetonitrile and 20% of water, under 0.8 ml/min flux). As expected, the most hydrophilic compound BDP2, is the one with the lowest retention time (t_R), while BDP5, the most aromatic compound, is the one with the highest t_R (ESI Fig. S1). All BODIPYs were synthesized with reasonable yields and isolated with a purity level above 99%.

Table 4
Photophysical properties of the BODIPY series.

Dyes	Solvent	λ^{abs} (nm)	ϵ ($\text{cm}^{-1} \text{M}^{-1}$)	λ^{abs} (nm) ^a	λ^{em} (nm)	ϕF	SS (cm^{-1})	$\Delta\lambda$ (nm)	$E_{\text{g}}^{\text{opt}}$ (eV) ^b
BDP1	Chloroform	525	6.8×10^4	548	538	98%	460	13	2.28
	Hexane	524	8.8×10^4		535	69%	388	11	2.28
	Acetonitrile	520	1.0×10^5		533	92%	468	13	2.29
BDP2	Chloroform	530	5.4×10^4	539	543	76%	452	13	2.25
	Hexane	526	6.4×10^4		539	73%	459	13	2.26
	Acetonitrile	523	6.9×10^4		537	71%	498	14	2.26
BDP3	Chloroform	544	5.9×10^4	551	558	98%	461	14	2.19
	Hexane	543	1.0×10^5		555	90%	398	12	2.19
	Acetonitrile	539	7.9×10^4		554	88%	502	15	2.21
BDP4	Chloroform	530	6.2×10^4	542	539	0.6%	315	9	2.25
	Hexane	530	8.6×10^4		549	28%	645	19	2.25
	Acetonitrile	526	7.8×10^4		534; 650	0.4%	284	8	2.27
BDP5	Chloroform	532	7.8×10^4	545	543	80%	209	13	2.26
	Hexane	528	9.6×10^4		538	77%	175	10	2.27
	Acetonitrile	527	5.9×10^4		537	67%	284	10	2.27
BDP6	Chloroform	533	6.2×10^4	538	539	84%	381	6	2.27
	Hexane	531	7.6×10^4		536	79%	352	5	2.27
	Acetonitrile	526	6.4×10^4		534	78%	254	8	2.29

^a Films prepared from chloroform and dichlorobenzene solution.

^b E_{g} = estimated from the absorption spectra onset of dyes in solution, E_{g} (eV) = $1240/\lambda_{\text{onset}}$ (nm).

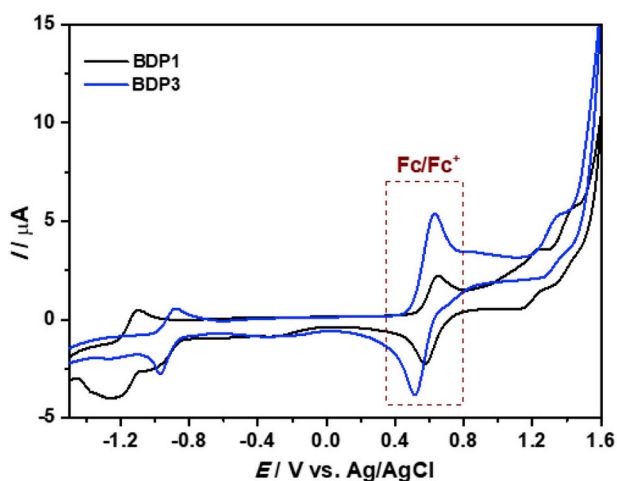


Fig. 2. Cyclic voltammograms of **BDP1** and **BDP3** in dichloroethane, containing 0.1 M TBATFB and 1 mM of the BODIPY compound in the presence of 1 mM ferrocene/ferrocenium (Fc/Fc^+) as internal standard, recorded at 50 mV s^{-1} in deoxygenated solution (N_2).

3.2. Anomalous meso-free BODIPY presence

In the synthesis of all *meso*-substituted BODIPYs (**BDP1-5**), the **BDP6** was isolated as a by-product in yields ranging from 2% to 6%. This peculiarity was already reported but never explained [28,29]. In

fact, the **BDP6** by-product can be easily masked by the main BODIPY in terms of visible spectroscopy, but by HPLC it is possible to identify both, and then isolate them, either by column chromatography or preparative thin layer chromatography. This contamination is particularly evident in the synthesis of **BDP1** and **BDP5**, having a direct influence on the lower yields of these BODIPYs due to the consumption competition of pyrrole units with the **BPD6** synthesis. Due to its almost identical photophysical properties, **BDP6** contamination must be taken seriously on photovoltaic studies, but this has not been referenced in almost all previously reported studies using BODIPYs made by the acid condensation of aldehydes and α -free-pyrroles.

We investigated the possibility of **BDP6** be the result of degradation of the main *meso*-substituted BODIPY products. A series of studies to evaluate the effect of several degradative factors, namely the temperature (room temperature and 50°C), light stability (under direct light or in the dark), the pH effect (under acidic conditions (1% of pure HCl) or under basic conditions (1% NaOH solution) and the oxidative conditions (1 equivalent of DDQ) or reductive conditions (1 equivalent of hydrazine) were performed. All experiments were continuously monitored (absorption spectroscopy and HPLC) for 24 h, and under no circumstances the formation of **BDP6** was detected. These preliminary results suggested that the formation of **BDP6** does not arise from the degradation of the *meso*-substituted BODIPYs (**BDP1-5**).

As an alternative hypothesis, we investigated the possibility of **BDP6** result from the reaction of the α -free-pyrrole with the solvent (CH_2Cl_2). Table 1 shows a few reaction conditions, all without the aldehyde reagent, to study the influence of the solvent on **BDP6** formation. In fact, it was possible to synthesize and isolate **BDP6** in the total

Table 5
Electrochemical properties of the six BODIPY compounds.

Dyes	E_{red}^1 (V)	E_{ox}^1 (V)	E_{ox}^2 (V)	$E_{\text{HOMO}}^{\text{ec}}$ (eV) ^a	$E_{\text{LUMO}}^{\text{ec}}$ (eV) ^b	E_{g}^{ec} (eV) ^c	$E_{\text{g}}^{\text{opt}}$ (eV) ^d	$E_{\text{LUMO}}^{\text{opt}}$ (eV) ^e
BDP1	-1.21	1.22	1.43	-5.35	-3.08	2.27	2.28	-3.07
BDP2	-1.16	1.24	1.43	-5.41	-3.12	2.29	2.25	-3.16
BDP3	-0.97	1.35	1.53	-5.50	-3.29	2.21	2.19	-3.31
BDP4	-1.25	1.12	1.38	-5.27	-2.99	2.28	2.25	-3.02
BDP5	-1.13	1.25	1.42	-5.39	-3.10	2.29	2.26	-3.13
BDP6	-1.13	1.22	1.39	-5.35	-3.08	2.27	2.27	-3.08

^a Estimated from the CV: $E_{\text{HOMO}} = [-(E_{\text{onset}}^{\text{ox1}} - E^{\text{Fc}/\text{Fc}^+}) - 4.8]$ eV.

^b Estimated from the CV: $E_{\text{LUMO}} = [-(E_{\text{onset}}^{\text{red1}} - E^{\text{Fc}/\text{Fc}^+}) - 4.8]$ eV.

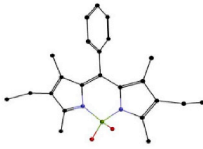
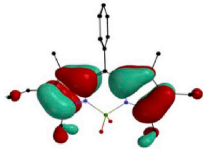
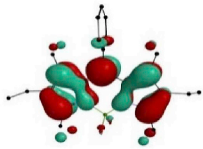
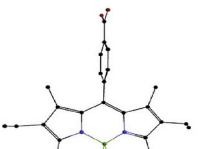
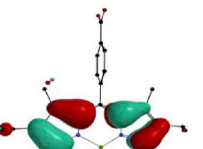
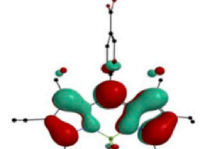
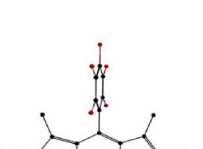
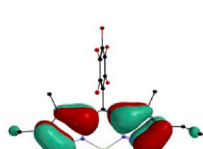
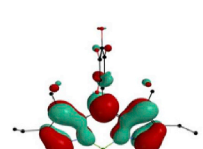
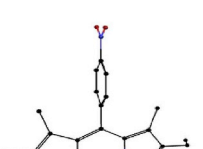
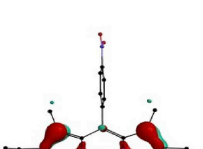
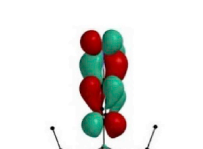
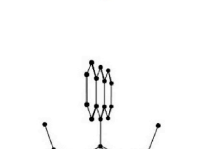
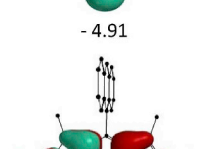
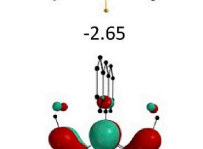
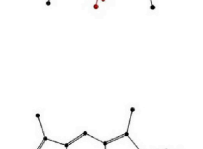
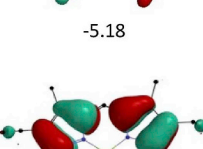
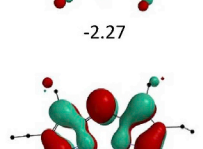
^c Estimated as the difference between the HOMO and LUMO obtained from CV measurements.

^d Estimated from the onset of absorption spectra in chloroform.

^e $E_{\text{LUMO}} = [E_{\text{HOMO}} + E_{\text{g}}^{\text{opt}}]$ eV.

Table 6

Optimized structures, electron distribution in HOMO and LUMO and their energies (in eV) of the BODIPY series, obtained by DFT calculations in vacuum.

BODIPY	Optimized Geometry	HOMO	LUMO
BDP1		 -5.16	 -2.24
BDP2		 -5.25	 -2.29
BDP3		 -5.42	 -2.62
BDP4		 -4.91	 -2.65
BDP5		 -5.18	 -2.27
BDP6		 -5.23	 -2.30

absence of aldehyde, which shows that the dichloromethane solvent is the source of the *meso*-carbon that leads to the unexpected formation of the *meso*-free BODIPY (**BDP6**). Under these conditions (absence of aldehyde), **BDP6** was the only BODIPY species formed. It was easily purified and isolated by column chromatography.

It was also found that the use of TFA as catalyst is not required, either because hydrochloric acid is formed *in situ* or because this aliphatic nucleophilic substitution reaction does not require acid catalysis. In summary, these preliminary results indicate that **BDP6** must arise from the reaction of pyrrole with the electrophilic carbon of the halogenated solvent and therefore future works must take this in consideration.

To further support our hypothesis of the dichloromethane role in the synthesis of **BDP6**, we performed the reaction of 3-ethyl-2,4-dimethylpyrrole with α,α -dichlorotoluene and α,α -dibromotoluene, and in

both cases we obtained exclusively the **BDP1** with 6% and 4% yield, respectively (Scheme 2). This result is consistent with previous studies of reaction of pyrrole with dihalogenated electrophiles reported in 1907 by Pictet and Rilliet [30], and the more recent reaction of pyrroles with a dihalogenated alkanes to synthesize corrole derivatives, by Gross et al. [31].

3.3. X-ray diffraction studies and the new structures

The crystallization of all BODIPYs was made through slow evaporation from a dichloromethane/hexane solution. We succeeded at obtaining crystals of **BDP3**, **BDP4**, **BDP5** and **BDP6**. Crystals of **BDP3** and **BDP6** exhibit a unit cell equal to that already reported by Rurack et al. [32] and Beniston et al. [29], respectively, with CCDC codenames FIDLIP and XODGUT.

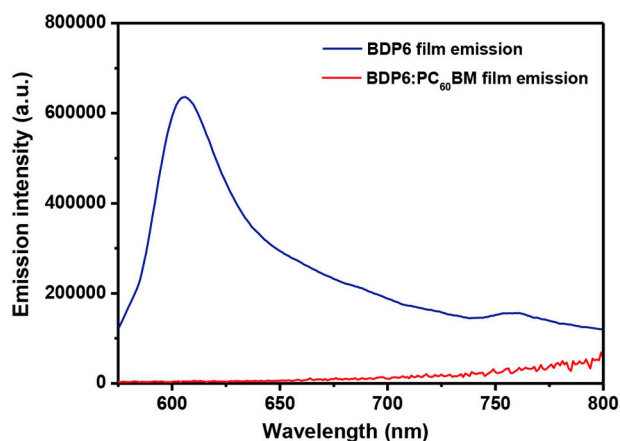


Fig. 3. Emission spectra of the films of BDP6 and BDP6:PC₆₀BM blend.

Table 7

Photovoltaic parameters from the BDP1-6:PC₆₀BM-based OPVs, under AM 1.5 G illumination at 88 mW/cm². All the solar cells were made under the optimized conditions for BDP6:PC₆₀BM solar cell (Table S2).

Dye	Active layer thickness (nm)	J _{sc} (mA/cm ²)	V _{oc} (V)	FF	Efficiency (%)	
					maximum	average ^a
BDP1	63	1.93	0.54	0.26	0.31	0.24
BDP3	110	0.09	0.42	0.26	0.01	0.009
BDP4	70	0.49	0.53	0.30	0.09	0.08
BDP5	63	1.55	0.62	0.27	0.30	0.26
BDP6	72	2.27	0.67	0.27	0.47	0.37

^a Average values calculated from at least 8 devices.

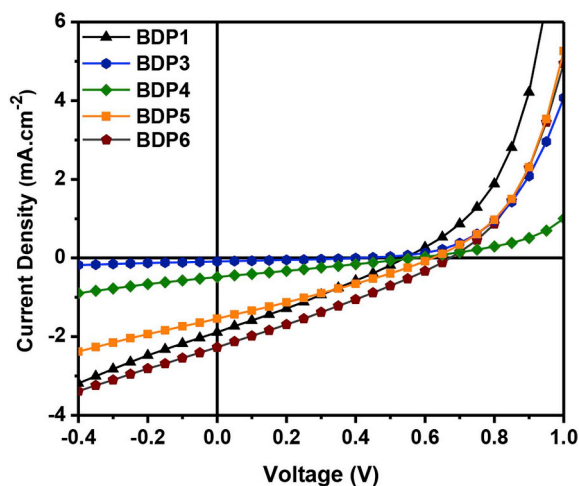


Fig. 4. Current density-voltage characteristics of BODIPY dyes:PC₆₀BM-based OPVs, under AM 1.5G illumination at 88 mW cm⁻².

In the case of BDP4, we have refined a new polymorph, different from that reported previously by Diederich et al. [33] (codename UNIFIG). We report here the first known crystal structure for BDP5. Table 2 shows the single-crystal X-ray structure of the BDP4 and BDP5 and crystal data details. Data collection and refinement data can be found in the supplementary information (Table S1).

BDP4 molecules, crystallize in a non-centrosymmetric unit cell in a triclinic space group. In UNIFIG, there are three symmetry-independent molecules while in the new polymorph (BDP4), reported here, there are only two. In UNIFIG, two molecules have the ethyl groups in a *trans*-conformation and the third one has the ethyl groups in a *cis*-conformation. The angles between the least-squares plane of the *meso*-substituent and the central planar molecular core are 78.9(2), 78.8(2)

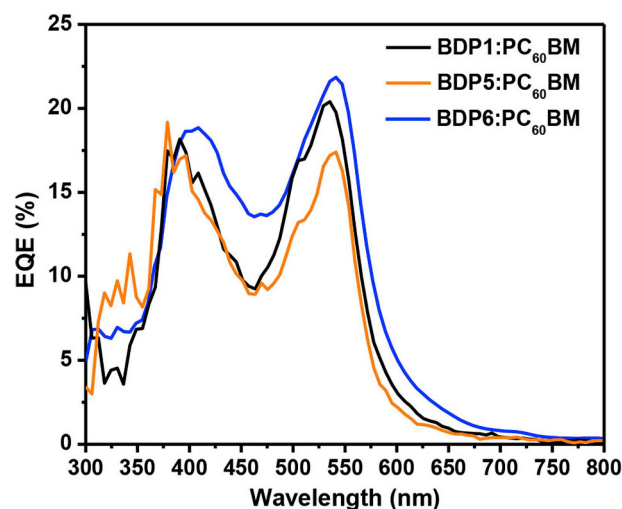


Fig. 5. EQE curves of the optimized BDP1:PC₆₀BM, BDP5:PC₆₀BM and BDP6:PC₆₀BM-based OPV cells.

and 84.5 (2)° for the three molecules. In the new polymorph, both molecules show a *trans*-conformation and the angle between the *meso*-substituent group and the core is 89.17 (6)° and 86.81 (7)°.

BDP5 crystallizes also in a triclinic unit cell with an inversion centre. The angle between the anthracene substituent and the central core of the molecule is 89.99 (5)°.

They pack efficiently without any solvent accessible voids (Table 3). Table 3 gathers information about BODIPY's angle and distance between the *meso*-carbon and the substituent carbon to which it is bonded.

3.4. Absorption and fluorescence spectroscopy

The absorption and emission spectra of all presented BODIPYs, in chloroform solution, are presented in Fig. 1 (A and B respectively), and the corresponding optical data is summarized in Table 4. The absorption spectra of BDP1-6 series cover a broad range of the visible spectrum. All six spectra are characterized by a strong S0-S1 (π - π^*) transition (525-544 nm) with a higher energy vibronic shoulder at about 30 nm from the main peak and a weaker broad band (340-420 nm) arising from the S0-S2 (π - π^*) transition. As it has been reported previously, the presence of an aromatic group at the *meso* position has a weak effect on the absorption/emission characteristics [15,17,28]. This is due to the negligible electronic interaction between the *meso*-aromatic ring and the BODIPY core, since the two moieties are almost perpendicular to each other. However, BDP3 presents a small red-shift if compared with the remaining members of the series, which can be explained by the inductive effect of the strong electron-withdrawing properties of the *meso*-C₆F₅ group.

Independently of the solvent, all BODIPY show high extinction coefficients (ranging from 5.4×10^4 to 1.0×10^5 cm⁻¹M⁻¹), which confirms their excellent light-harvesting ability.

Apart from BDP4, the various BODIPY dyes present high fluorescence quantum yields, and their emission spectra are mirror images of the S0-S1 transition of the absorption spectra. Excitation spectra match the absorption spectra allowing us to conclude that the emitted light originates from the singlet excited state without any contribution of any charge transfer or other excited state. The small Stokes shift is a typical characteristic of these compounds, and it is an indication of a similar S1 and S0 configuration.

The emission of BDP4 (p-nitro-phenyl substituted BODIPY) is significantly affected by solvent polarity. In hexane, it shows fluorescence emission (at 549 nm) but in chloroform the fluorescence quantum yield becomes very weak, and in acetonitrile the fluorescence quantum yield

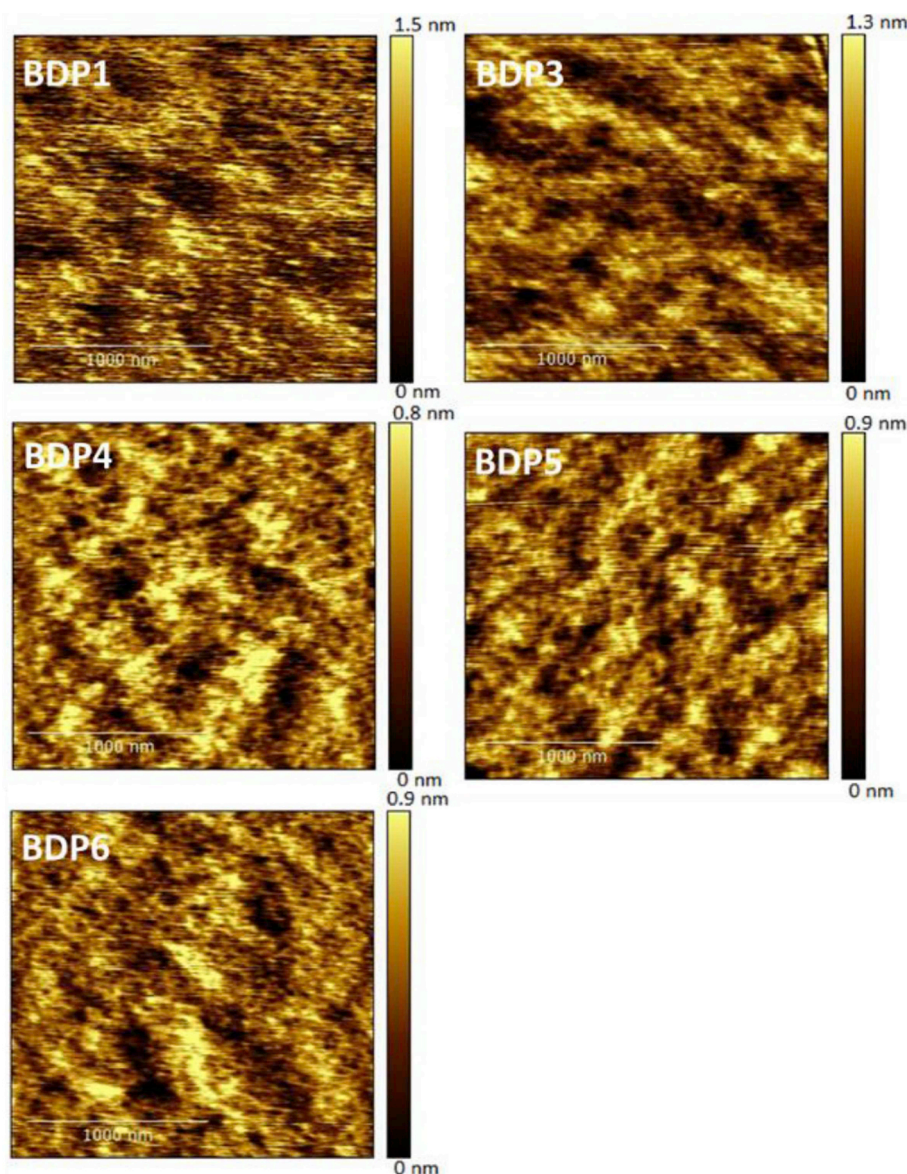


Fig. 6. AFM topography images (2 μm vs 2 μm) of **BDP1**: PC₆₀BM (RMS:0.38 nm), **BDP3**:PC₆₀BM (RMS:0.30 nm), **BDP4**: PC₆₀BM (RMS:19 nm), **BDP5**: PC₆₀BM (RMS:0.23 nm), **BDP6**: PC₆₀BM (RMS:0.21 nm).

becomes residual and a new band at 650 nm arises (Fig. 1 (C)). The quenching of the emission in polar media and the appearance of new red-shifted bands are usually associated with the formation of intramolecular charge transfer (CT) states [34]. Thus, the **BDP4** emission in polar solvents can be rationalized as a mixture of local fluorescence and CT excited states, formed from intramolecular electron transfer.

The absorption spectra of the BODIPY thin films show a clear bathochromic shift of the absorption maximum accompanied by a broadening of the peaks (Fig. S27), due to the interactions between adjacent molecules, possibly involving π -orbitals.

3.5. Electrochemical properties

Cyclic voltammetry (CV) was used to study the electrochemical properties of the BODIPY dyes in the presence of 0.1 M TBATFB in dichloroethane, as supporting electrolyte. The ferrocene/ferrocenium (Fc/Fc⁺) couple was used as internal reference and it is assumed that the redox potential of Fc/Fc⁺ has an absolute energy level of 4.80 eV in relation to vacuum. Solutions were degassed with N₂ for 5 min before CV measurements. Fig. 2 illustrates the cyclic voltammograms of **BDP1**

and **BDP3** (all cyclic voltammograms can be found in the support information (Figs. S28–S33)). The electrochemical properties of all these BODIPYs are summarized in Table 5.

All BODIPYs present quasi-reversible redox processes with very similar cyclic voltammograms, with two oxidations processes (E_{ox}^1 and E_{ox}^2) and one reduction process (E_{red}^1). These processes can be assigned almost exclusively to the BODIPY core, not only because the HOMO of *meso*-BODIPY dyes is generally delocalized over the BODIPY core.

BDP3 oxidation and reduction potentials are slightly shifted to more positive potentials, which can be attributed to the stabilization effect of the pentafluoro withdrawing groups.

The HOMO and LUMO energy levels were calculated using the onset of the first oxidation peak and the first reduction peak respectively. The LUMO energies were also calculated using the optical energy gap (Table 4) as reported by several authors [21,35–38]. The differences between the LUMO energies and energy gaps obtained from cyclic voltammetry and those calculated from the optical energy-gap are minimal or non-existent.

The calculated HOMO and LUMO energies indicate that all six BODIPYs are suitable candidates to be used as electron-donors with

respect to PC₆₀BM in BHJ photovoltaic cells because their HOMO and LUMO lie above the corresponding levels of PC₆₀BM i.e. -6.1 eV and -3.7 eV, respectively, thereby forming a type II heterojunction.

3.6. Theoretical calculations

To better understand the change of photophysical and electrochemical properties among the various BODIPYs, the structures and energies of the frontier orbitals were calculated by Density Functional Theory (DFT) in vacuum. The optimized ground-state geometries and electronic distribution in HOMO-LUMO levels are presented in Table 6. All calculations were carried out using the B3LYP method and a 6–31 G* basis set.

The six-member ring of BODIPY core is almost planar. Around the boron atom, in a tetrahedral coordination, the two fluorine atoms are perpendicular to the BODIPY core. The *meso*-substituted groups are nearly perpendicular to the plane of the BODIPY core.

The π -electrons in the HOMOs are delocalized over the entire BODIPY backbone π -systems. Similarly, the LUMO orbitals in all BODIPYs, with the exception of **BDP4**, are delocalized also within the BODIPY backbone but with higher intensity at the *meso* carbon. Due to the less perpendicular symmetry of *meso* group on **BDP3** there is a very small delocalization between the backbone and the *meso*-substituting group. In the case of **BDP4**, the LUMO is entirely localised in the nitrophenyl substituent. The absence of spatial overlap between HOMO and LUMO of **BDP4**, indicates that the HOMO – LUMO transition has a charge transfer character, which is in line with the fluorescence results discussed above.

The HOMO energies obtained from cyclic voltammetry are very similar to the theoretical ones. However, a somewhat higher deviation is found for the LUMO energy. The dissimilarity between the experimental LUMO energy and the calculated can be justified by the lack of solvent stabilisation effects. Nevertheless, the experimental and calculated data follows the same trend, in what concerns HOMO, LUMO and energy-gap, and confirm that all the six BODIPYs are suitable candidates to be used as electron donors in OPVs when blended with PC₆₀BM.

3.7. Photovoltaic performance evaluation and surface morphology

All BODIPYs exhibit the fundamental requirements to be used as electron-donor materials in PC₆₀BM-based OPVs. Fluorescence studies of the film prepared with the **BDP6**:PC₆₀BM blend (Fig. 3) reveal a complete quenching of the BODIPY emission, which is consistent with an excited state electron transfer from BODIPY to fullerene, thereby providing good perspectives for application in OPVs.

Solution-processed bulk heterojunction OPVs were manufactured with a typical multilayer structure: ITO/PEDOT:PSS/active layer/LiF/Al. The PEDOT:PSS layer was spin-coated at 1800 rpm and dried for 10 min at 125 °C to obtain a film thickness of about 40 nm. Several conditions of the active layer were tested, aiming to achieve the best power conversion efficiency (PCE). The optimization procedures, Table S2 (Supplementary Information), were carried out with **BDP6**-based devices and then replicated in the OPVs based on the remaining BODIPYs. The adjusted parameters were: donor/acceptor weight ratio, active layer solution concentration and back (top) electrode (Ca/Al or LiF/Al).

The optimized **BDP6**-based OPV was prepared from a **BDP6**:PC₆₀BM blend with a weight ratio of 1:3, dissolved in dichlorobenzene at 40 mg/ml, and deposited by spin-coating at 1200–1300 rpm with LiF/Al top electrode.

Devices based on **BDP2** were poorly characterized due to the **BDP2** low solubility, which led to films with poor quality and irregular current-voltage (J–V) curves. For this reason, **BDP2** was not included in the photovoltaic studies.

The parameters characterizing the photovoltaic cells performance are given in Table 7 and the J–V curves are shown in Fig. 4. For the optimized conditions, the best PCE values were obtained with the

BDP6-based devices. Devices based on **BDP1** and **BDP5** showed a slightly lower efficiencies. **BDP3** and **BDP4** led to OPV with much worst performance. The current density versus voltage, in the dark and under illumination, for the best BODIPYs:PC₆₀BM cells are shown in the supplementary information (Fig. S34).

As mentioned above, the optimization process showed that the best thickness of the active layer should be around 70 nm. However, under the optimal conditions, **BDP3** has 110 nm of active layer thickness. When the active layer thickness was reduced to 77 nm (using 35 mg/ml solution concentration) the PCE remained at 0.01%. The thinner layer caused a small increase in short circuit current (J_{SC}) but also a decrease of open circuit voltage (V_{OC}).

The presented BODIPY-based OPVs show high V_{OC} values, some of which are similar to those of the best BODIPY-based solar cells, but the main limitation factors in these systems are J_{SC} and fill factor (FF). These parameters are related to light harvesting ability, recombination, charge transport and collection. Since the proposed BODIPY dyes show high absorption coefficients and absorbance in a favourable range of the spectrum, we believe that the main restriction of this system is related to a non-optimal active layer morphology or to a poor charge transport.

Among the five tested BODIPYs, the largest difference between the corresponding devices is in the current. The best BODIPY is the one with the free-*meso*-position and the worst (**BDP3** and **BDP4**) are the BODIPYs with electron-withdrawing groups at the *meso*-position. These results show that the nature of the group at the *meso* position significantly affects the photovoltaic performance. Since the *meso* group is perpendicular to the BODIPY core and it does not have a considerable influence on the optical-electronics properties, the differences in device performance are likely related to the intermolecular interactions and molecular packing.

The external quantum efficiencies (EQE) were also measured for **BDP1**:PC₆₀BM, **BDP5**:PC₆₀BM, **BDP6**:PC₆₀BM (Fig. 5). The EQE profiles are similar to the corresponding absorption spectra of the films, with a broad response in the 375–600 nm range. This response is mainly due to the BODIPY absorption profile but some contribution of PC₆₀BM at 300–400 nm is also detected. The stronger response of the **BDP6**-based OPV is consistent with a higher short-circuit current.

The morphology of the OPVs' active layers can provide valuable information about the photoelectronic response, being related with exciton dissociation efficiency and, consequently, with the obtained photocurrent. For that reason, the film's surface of **BDP1**:PC₆₀BM, **BDP3**:PC₆₀BM, **BDP4**:PC₆₀BM, **BDP5**:PC₆₀BM and **BDP6**:PC₆₀BM were characterized by AFM (Fig. 6 and Fig. S35). All films exhibit very similar surface topography without noticeable phase domains or aggregates. They are very flat (root mean squared (RMS) inferior to 0.40 nm). Usually low roughness and small phase domains are indicators of good miscibility between the donor and the acceptor and are associated with good photovoltaic efficiencies. These results demonstrate that there is a good miscibility between the BODIPY dyes and the PC₆₀BM, with a good donor:acceptor interpenetrating network within the blend films.

The AFM results show a good intermixing of the two active layer materials (BODIPY and PCBM). This morphology facilitates the exciton dissociation (by virtue of a large donor/acceptor interface) but tends to limit the charge transport, as it does not allow the formation of percolation paths for the generated charges to reach the electrodes.

The hole mobility in films of neat BODIPYs was calculated from the current-voltage characteristics of hole-only devices, with the structure ITO/PEDOT:PSS/BODIPY/MoO₃/Al in the space charge limited current (SCLC) regime [39]. The calculated values were **BDP1**: 3×10^{-7} cm²/V.s; **BDP3**: 6×10^{-6} cm²/V.s; **BDP4**: 6×10^{-7} cm²/V.s; **BDP6**: 1×10^{-6} cm²/V.s. In case of **BDP5**, we could not observe such SCLC regime, and the mobility could not be calculated using this method. Despite the similarity of the calculated mobilities to some reported BODIPY-based OPVs [40,41], these values are much lower than both

values we obtained, by the same method, for P3HT ($2 \times 10^{-3} \text{ cm}^2/\text{V.s}$) and the electron mobility reported in PCBM ($4 \times 10^{-3} \text{ cm}^2/\text{V.s}$) [39]. These results suggest that the hole mobility in the BODIPY phase does limit the performance of the OPVs.

4. Conclusions

In this work we report the synthesis and characterization of a series of simple *meso*-BODIPY molecules, as well as two new crystal structures. We showed that the synthesis of the unexpected *meso*-free-BDP6 results from the reaction of the pyrrole with the solvent (dichloromethane). Therefore, the use of halogenated solvents in these reactions implies a rigorous evaluation of by-products. But equally important those studies show that we can produce BODIPYs by aliphatic nucleophilic substitution over halogenated molecules. Despite being a reaction that is more than a century old, it was never exploited in BODIPY chemistry and our results show that it may be a valuable alternative to acid sensitive BODIPY targets.

From our studies some noticeable effects on the photovoltaic properties can be drawn. The best photovoltaic performance was obtained with BDP6 (BODIPY without *meso* groups), pointing to the fact that the substitution at this position can negatively influence the photovoltaic cells efficiency. Among the *meso*-substituted BODIPYs, BDP1 (phenyl group at the *meso* position) and BDP5 (anthracyl group at *meso* position) have a similar photovoltaic response, and they are around 3 times better than BDP4 (*para*-nitrophenyl group at *meso* position) and 27 times better than BDP3 (pentafluorophenyl group at the *meso* position). This variation indicates that the strong electron withdrawing groups at *meso*-position can cause large drop in OPV performance. Despite the low hole mobility, the V_{OC} of our tested BODIPY-based OPV cells are comparable to the values of some of the best OPV cells. The AFM studies of the active layer blend show a very good miscibility between our tested BODIPYs and PC₆₀BM, with the blend films showing very flat surfaces. These results can be used as standard results for validation of further BODIPYs functionalization and their application in photovoltaics.

Acknowledgements

The authors acknowledge Fundação para a Ciência e a Tecnologia (FCT), Portuguese Agency for Scientific Research, for the PhD research grant PD/BD/113702/2015, the postdoctoral grant SFRH/BPD/86507/2012 and CNPq, Brazil for PhD research grant 232979/2014-6. The work at “The Coimbra Chemistry Centre” is funded by FCT, through the projects FCT UID/QUI/UI0313/2013 and COMPETE Programme (Operational Programme for Competitiveness). The work at IT is funded by FCT/MEC through national funds and when applicable co-funded by FEDER – PT2020 partnership agreement under the project UID/EEA/50008/2019.

Appendix A. Supplementary data

Supplementary data to this article can be found online at <https://doi.org/10.1016/j.dyepig.2019.107842>.

References

- [1] Kumar P. Organic solar cells: device physics, processing, degradation, and prevention. CRC Press, Taylor & Francis Group; 2017.
- [2] Jäger-Waldau A. Photovoltaics: status and perspectives until 2020. Green2011. p. 277.
- [3] Tian H, Sun L. 8.16 - organic photovoltaics and dye-sensitized solar cells. In: Reedijk J, Poepelmeier K, editors. Comprehensive inorganic chemistry II. second ed. Amsterdam: Elsevier; 2013. p. 567–605.
- [4] Hoth CN, Schilinsky P, Choulis SA, Brabec CJ. Printing highly efficient organic solar cells. Nano Lett 2008;8(9):2806–13.
- [5] Scharber MC, Sariciftci NS. Efficiency of bulk-heterojunction organic solar cells. Prog Polym Sci 2013;38(12):1929–40.
- [6] Yeh N, Yeh P. Organic solar cells: their developments and potentials. Renew Sustain Energy Rev 2013;21:421–31.
- [7] Chen Y, Wan X, Long G. High performance photovoltaic applications using solution-processed small molecules. Accounts Chem Res 2013;46(11):2645–55.
- [8] Durantini AM, Heredia DA, Durantini JE, Durantini EN. BODIPYs to the rescue: potential applications in photodynamic inactivation. Eur J Med Chem 2018;144:651–61.
- [9] Bessette A, Hanan GS. Design, synthesis and photophysical studies of dipyrromethene-based materials: insights into their applications in organic photovoltaic devices. Chem Soc Rev 2014;43(10):3342–405.
- [10] Bucher L, Desbois N, Harvey PD, Sharma GD, Gros CP. Porphyrins and BODIPY as building blocks for efficient donor materials in bulk heterojunction solar cells. Solar Rrl 2017;1(12).
- [11] Rumin J, Bonnefond H, Saint-Jean B, Rouxel C, Sciandra A, Bernard O, et al. The use of fluorescent Nile red and BODIPY for lipid measurement in microalgae. Biotechnol Biofuels 2015;8:42.
- [12] Zhang J, Zhao B, Li C, Zhu X, Qiao R. A BODIPY-based “turn-on” fluorescent and colorimetric sensor for selective detection of Cu²⁺ in aqueous media and its application in cell imaging. Sens Actuators B Chem 2014;196:117–22.
- [13] Zampetti A, Minotto A, Squeo BM, Gregoriou S, Allard S, Scherf U, et al. Highly efficient solid-state near-infrared organic light-emitting diodes incorporating A-D-A dyes based on α,β -unsubstituted “BODIPY” moieties. Sci Rep 2017;7(1):1611.
- [14] Gabe Y, Urano Y, Kikuchi K, Kojima H, Nagano T. Highly sensitive fluorescence probes for nitric oxide based on boron dipyrromethene Chromophore Rational design of potentially useful bioimaging fluorescence probe. J Am Chem Soc 2004;126(10):3357–67.
- [15] Loudet A, Burgess K. BODIPY dyes and their derivatives: syntheses and spectroscopic properties. Chem Rev 2007;107(11):4891–932.
- [16] Klifout H, Stewart A, Elkhalfi M, He H. BODIPYs for dye-sensitized solar cells. ACS Appl Mater Interfaces 2017;9(46):39873–89.
- [17] Ulrich G, Ziesler R, Harriman A. The chemistry of fluorescent bodipy dyes: versatility unsurpassed. Angew Chem Int Ed 2008;47(7):1184–201.
- [18] Rousseau T, Cravino A, Bura T, Ulrich G, Ziesler R, Roncali J. BODIPY derivatives as donor materials for bulk heterojunction solar cells. Chem Commun 2009(13):1673–5.
- [19] Srinivasa Rao R, Bagui A, Hanumantha Rao G, Gupta V, Singh SP. Achieving the highest efficiency using a BODIPY core decorated with dithiafulvalene wings for small molecule based solution-processed organic solar cells. Chem Commun 2017;53(51):6953–6.
- [20] Liao J, Xu Y, Zhao H, Zong Q, Fang Y. Novel A-D-A type small molecules with β -alkynylated BODIPY flanks for bulk heterojunction solar cells. Org Electron 2017;49:321–33.
- [21] Liao J, Zhao H, Xu Y, Cai Z, Peng Z, Zhang W, et al. Novel D–A–D type dyes based on BODIPY platform for solution processed organic solar cells. Dyes Pigments 2016;128:131–40.
- [22] Zhao H, Wang B, Liao J, Wang H, Tan G. Synthesis, spectral, electrochemical properties, and photovoltaic performance of structurally constrained BODIPY dyes with 4,4-dimethyltriphenylamine at the 2,6-positions. Tetrahedron Lett 2013;54(45):6019–22.
- [23] Misra R, Jadhav T, Dhokale B, Gautam P, Sharma R, Maragani R, et al. Carbazole-BODIPY conjugates: design, synthesis, structure and properties. Dalton Trans 2014;43(34):13076–86.
- [24] SAINT plus data reduction and correction program va. Madison, Wisconsin: Bruker AXS; 2003.
- [25] Sheldrick S GM. Germany: University of Gottingen; 1996.
- [26] Sheldrick G. Crystal structure refinement with SHELXL. Acta Crystallogr C 2015;71(1):3–8.
- [27] Arranja CT, Aguiar A, Encarnação T, Fonseca SM, Justino LLG, Castro RAE, et al. Double-tailed long chain BODIPYs - synthesis, characterization and preliminary studies on their use as lipid fluorescence probes. J Mol Struct 2017;1146:62–9.
- [28] Banfi S, Nasini G, Zaza S, Caruso E. Synthesis and photo-physical properties of a series of BODIPY dyes. Tetrahedron 2013;69(24):4845–56.
- [29] Benniston AC, Copley G, Elliott KJ, Harrington RW, Clegg W. Redox-controlled fluorescence modulation in a BODIPY-quinone dyad. Eur J Org Chem 2008;2008(16):2705–13.
- [30] Pictet A, Rilliet A. Über die Einwirkung von Formaldehyd und von Methylenchlorid auf Pyrrol. Ber Dtsch Chem Ges 1907;40(1):1166–72.
- [31] Chen Q-C, Soll M, Mizrahi A, Saltsman I, Fridman N, Saphier M, et al. One-pot synthesis of contracted and expanded porphyrins with *meso*-CF₃ groups. Angew Chem Int Ed 2018;57(4):1006–10.
- [32] Hecht M, Fischer T, Dietrich P, Kraus W, Descalzo AB, Unger WES, et al. Fluorinated boron-dipyrromethene (BODIPY) dyes: bright and versatile probes for surface analysis. ChemistryOpen 2013;2(1):25–38.
- [33] Azov VA, Skinner PJ, Yamakoshi Y, Seiler P, Gramlich V, Diederich F. Functionalized and partially or differentially bridged resorcin[4]arene cavitands: synthesis and solid-state structures. Helv Chim Acta 2003;86(11):3648–70.
- [34] Maus M, Rettig W, Bonafoux D, Lapouyade R. Photoinduced intramolecular charge transfer in a series of differently twisted Donor–Acceptor biphenyls as revealed by fluorescence. J Phys Chem A 1999;103(18):3388–401.
- [35] Kubo Y, Watanabe K, Nishiyabu R, Hata R, Murakami A, Shoda T, et al. Near-Infrared absorbing boron-dibenzopyrromethenes that serve as light-harvesting sensitizers for polymeric solar cells. Org Lett 2011;13(17):4574–7.
- [36] Zou L, Guan S, Li L, Zhao L. Dipyrin-based complexes for solution-processed organic solar cells. Chem Res Chin Univ 2015;31(5):801–8.
- [37] Poe AM, Della Pelle AM, Subrahmanyam AV, White W, Wantz G, Thayumanavan S. Small molecule BODIPY dyes as non-fullerene acceptors in bulk heterojunction

- organic photovoltaics. *Chem Commun* 2014;50(22):2913–5.
- [38] Bura T, Leclerc N, Fall S, Lévêque P, Heiser T, Retailleau P. High-performance solution-processed solar cells and ambipolar behavior in organic field-effect transistors with thienyl-BODIPY scaffoldings. *J Am Chem Soc* 2012;134(42):17404–7.
- [39] Mihailetschi VD, Wildeman J, Blom PWM. Space-charge limited photocurrent. *Phys Rev Lett* 2005;94(12). 126602.
- [40] Kim B, Ma B, Donuru VR, Liu H, Fréchet MJM. Bodipy-backboned polymers as electron donor in bulk heterojunction solar cells. *Chem Commun* 2010;46(23):4148–50.
- [41] Rousseau T, Cravino A, Bura T, Ulrich G, Ziessel R, Roncali J. BODIPY derivatives as donor materials for bulk heterojunction solar cells. *Chem Commun* 2009(13):1673–5.